

Isotherm model for hightemperature, high-pressure adsorption of CO2 and H2O on K-promoted hydrotalcite

J. Boon (ECN) P.D. Cobden (ECN) H.A.J. van Dijk (ECN) C. Hoogland (ECN) E.R. van Selow (ECN) M. van Sint Annaland (TU/e) November 2014 ECN-W--14-003

ELSEVIER

Contents lists available at ScienceDirect

Chemical Engineering Journal

journal homepage: www.elsevier.com/locate/cej

Chemical Engineering Journal

Isotherm model for high-temperature, high-pressure adsorption of CO₂ and H₂O on K-promoted hydrotalcite



Jurriaan Boon a,b,*, P.D. Cobden A, H.A.J. van Dijk A, C. Hoogland E.R. van Selow M. van Sint Annaland b

HIGHLIGHTS

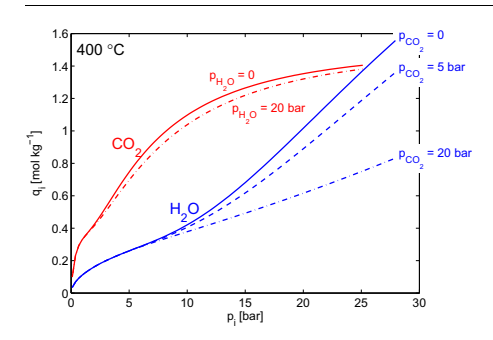
- We measured breakthrough curves for CO_2 and H_2O adsorption at $400\,^{\circ}C$, up to 24 bar.
- \bullet Surface adsorption occurs at specific sites for CO $_2$ or H_2O up to 5 bar.
- CO₂ and H₂O adsorb competitively in nanopores at higher partial pressures.
- Adsorption isotherm and sorption kinetics have been validated with a reactor model.

ARTICLE INFO

Article history:
Received 31 January 2014
Received in revised form 12 March 2014
Accepted 15 March 2014
Available online 26 March 2014

Keywords:
CO₂ adsorption
H₂O adsorption
Sorption-enhanced water-gas shift
Potassium-promoted hydrotalcite
Adsorption isotherm
Linear driving force

G R A P H I C A L A B S T R A C T



ABSTRACT

Sorption-enhanced water-gas shift (SEWGS) combines the water-gas shift reaction with in situ adsorption of CO_2 on potassium-promoted hydrotalcite (K-HTC) and thereby allows production of hot, high pressure H_2 from syngas in a single process. SEWGS is a cyclic process, that comprises high pressure adsorption and rinse, pressure equalisation, and low pressure purge. In order to design the SEWGS process, the equilibria and kinetics of adsorption must be known for the entire pressure range. Here, a multicomponent adsorption isotherm is presented for CO_2 and H_2O on K-HTC at $400\,^{\circ}C$ and 0.5–24 bar partial pressure, that has been derived from integrated experimentally determined breakthrough curves with special attention being given to the high pressure interaction. The experimental results can be well described by assuming that the isotherm consists of a low partial pressure surface adsorption part and a high partial pressure nanopore adsorption part. Surface adsorption occurs at specific and different sites for CO_2 or H_2O . In contrast, the nanopore adsorption mechanism is competitive and explains the interaction observed in the capacity data at partial pressures over 5 bar. Based on the characteristics of the sorbent particles, a linear driving force relation has been derived for sorption kinetics. Adsorption isotherm and linear driving force kinetics have been included in a reactor model. Model predictions are in agreement with breakthrough as well as regeneration experiments.

© 2014 Elsevier B.V. All rights reserved.

1. Introduction

In sorption-enhanced water–gas shift (SEWGS), the water–gas shift (WGS) reaction (1) is combined with in situ adsorption of CO₂ (2), typically at about 400 °C).

$$CO + H_2O = CO_2 + H_2 \quad \Delta H_{298 \text{ K}}^{\circ} = -41 \text{ kJ mol}^{-1}$$
 (1)

$$CO_2 + \bullet = CO_2 - \bullet$$
 (2)

Fed with syngas at temperatures in the range of 300–500 °C, potassium promoted hydrotalcite (K-HTC) catalyses the WGS reaction (1) and is capable of reversibly adsorbing CO_2 , thus finding use as sorbent in the SEWGS process [1–3]. The CO_2 is released during periodic regeneration of the K-HTC and the process comprises multiple reactors which are operated in pressure cycles, resembling

^a Sustainable Process Technology, ECN, P.O. Box 1, 1755ZG Petten, The Netherlands

^b Chemical Process Intensification, TU/e, P.O. Box 513, 5600MB Eindhoven, The Netherlands

^{*} Corresponding author at: Sustainable Process Technology, ECN, P.O. Box 1, 1755ZG Petten, The Netherlands. Tel.: +31 224564576; fax: +31 224568487. E-mail address: boon@ecn.nl (J. Boon).

Nomenclature Α nanopore-sorbate interaction parameter. – water-gas shift reaction rate, mol kg⁻¹ s⁻¹ r_{WGS} a_p particle interfacial area per unit volume, m⁻¹ T temperature, K molar concentration (= $\rho \omega_i / M_i$), mol m⁻³ С time, s concentration at the gas phase-particle interface, time of complete breakthrough, s c_{int} $mol m^{-3}$ T_c critical temperature. K particle heat capacity, J $\mathrm{kg^{-1}}\ \mathrm{K^{-1}}$ T_w wall temperature, K gas heat capacity, J kg⁻¹ K⁻¹ U overall heat transfer coefficient, W m⁻² K⁻¹ C_p particle diameter, m superficial gas velocity, m s⁻¹ d_p и d_r interstitial gas velocity, m s⁻¹ reactor internal diameter, m ν D_7 axial mass dispersion coefficient, m² s⁻¹ v_m molar volume, cm³ mol⁻¹ effective intraparticle molar diffusion coefficient, m² s⁻¹ \mathcal{D}_n limiting nanopore volume per mass of sorbent, V_0 Е nanopore-sorbate interaction energy, J mol⁻¹ cm3 kg f friction factor, - V_g interparticle and intraparticle gas volume in the colmolar flow rate, $mol \ s^{-1}$ umn, m³ adsorption enthalpy, $J \text{ mol}^{-1}$ ΔH_a mole fraction of species i, – y_i reaction enthalpy water-gas shift, I mol⁻¹ ΔH_r species index, -Greek surface-sorbate interaction parameter, Pa⁻¹ Κ bed porosity, - ϵ_b $k_{\rm LDF}$ linear driving force intraparticle mass transfer coeffiparticle porosity, - ϵ_p cient, s⁻¹ axial thermal conductivity, W m⁻¹ K⁻¹ molar mass, kg mol⁻¹ M mass fraction, ω pore-size distribution parameter, gas density, $kg m^{-3}$ m ρ m_s sorbent mass, kg particle density, kg m⁻³ ρ_p Freundlich isotherm parameter, molar flux, mol m⁻² s⁻¹ N **Abbreviations** Ν total number of species, -HTC hydrotalcite pressure, Pa р K-HTC potassium-promoted hydrotalcite p_c critical pressure, Pa pressure swing adsorption **PSA** saturation pressure, extrapolated to $T > T_c$, Pa p_0 **SEWGS** sorption-enhanced water-gas shift excess amount adsorbed, mol kgq standard litre per minute, gas volume defined at slpm $q^{\rm eq}$ equilibrium amount adsorbed, mol kg⁻¹ 273.15 K and 101,325 Pa maximum (monolayer) amount adsorbed, mol kg⁻¹ q^s WGS water-gas shift gas constant, J mol⁻¹ K⁻¹ R

the cycles of a pressure swing adsorption (PSA) process. Thus, the overall process directly converts syngas into separate streams of $\rm H_2$ and $\rm CO_2$ at 400 °C, which makes the SEWGS process exceptionally suitable for precombustion $\rm CO_2$ capture mitigating greenhouse gas emissions [4–6]. Design of the SEWGS process, as for any adsorption process, inherently relies heavily upon a reliable description of the relevant sorption equilibrium and kinetics.

Sorption of CO₂ on HTC has been extensively studied at relevant temperatures, but predominantly at relatively low pressures, Sorption of H₂O on K-HTC has not been quantified under relevant conditions, although the effect of steam upon CO₂ adsorption has been addressed qualitatively. Ding and Alpay [7] were the first to publish high temperature adsorption isotherms for CO₂ on K-HTC. A Langmuir adsorption isotherm was fitted with a maximum capacity of 0.65 mol kg⁻¹ for CO₂ partial pressures up to 0.6 bar and in the presence of water vapour; an approximately 10% lower capacity was found for dry conditions. The heat of adsorption was estimated at 17 kJ mol⁻¹. The capacity for CO₂ was found to be insensitive to the actual concentration of feed water for steam partial pressures between 0.03 and 2.45 bar. Some irreversible adsorption has been reported during the first contact of fresh K-HTC with CO₂. More recently, Lee et al. [8] measured CO₂ dry adsorption up to 3 bar partial pressure. They found that a Langmuir isotherm with a monolayer capacity of 0.25 mol kg⁻¹ could describe the equilibrium for low partial pressures. For CO₂ partial pressures over 0.2 bar, additional surface complexes are assumed to be formed, leading to a capacity of 0.87 mol kg⁻¹ at 3 bar partial pressure. Oliveira et al. [9] tested the CO₂ capacity of a series of

K-HTC's with varying Mg:Al ratio, in the presence of steam. Designating their samples as K-MGx, where x represents the weight percentage of MgO in the total amount of MgO and Al₂O₃, K-MG30 had a capacity of 0.76 mol kg⁻¹, compared to 0.6 mol kg⁻¹ for K-MG50 and 0.5 mol kg⁻¹ for K-MG70, all at a CO₂ partial pressure of 0.4 bar. Halabi et al. [10] used breakthrough measurements with 0.1-8.5 bar of CO₂ in the presence of 0.24 bar steam in order to derive sorption capacities of K-MG60 up to 0.97 mol kg⁻¹. A Freundlich isotherm was fitted to their data. Alternatively, approaching the sorption of CO₂ on HTC from a chemical kinetic point of view, Ebner et al. [11,12] measured 'nonequilibrium isotherms' for K-HTC at CO₂ partial pressures between 0.09 and 1.31 bar in absence of steam, reporting a rapid initial uptake, followed by slow sorption kinetics leading to a complex reaction pathway comprising three coupled reversible reactions. The maximum CO₂ capacity measured was 1.6 mol kg⁻¹. Wu et al. [13] recently measured a CO₂ capacity of up to $1.13\,\mathrm{mol\,kg^{-1}}$ for K-MG30 at $0.5\,\mathrm{bar}$ CO₂ and 0.5 bar H₂O, where a bi-Langmuir isotherm accounting for chemisorption and physisorption contributions could describe the data. Much higher capacities of up to 15 mol kg⁻¹ have been reported at high partial pressures of both CO2 and H2O and depending on the composition of the HTC [14,15]. These values, however, are attributed to the formation of bulk MgCO₃, which is relatively slow and undesirable for pressure-swing SEWGS operation. Van Selow et al. [4] have linked the formation of bulk MgCO₃ to CO₂ slip and loss of mechanical integrity. For the adsorption of H₂O on K-HTC, van Selow et al. [16] have proposed Langmuir isotherm, assuming a single adsorption site specific for H₂O. Thus, in spite of many papers addressing the reversible adsorption of CO_2 on K-HTC, crucial data is lacking for a well-founded SEWGS process design. The data for CO_2 adsorption is limited to a CO_2 partial pressure up to 8.5 bar, while in practice it may reach higher values. More importantly, the effect of steam upon the adsorption of CO_2 has not been quantified. Finally, the adsorption isotherm of H_2O on K-HTC itself has not been quantified.

Breakthrough experiments with CO_2 and H_2O provide an opportunity to measure relevant adsorption isotherms on K-HTC. Experiments with either CO_2 or H_2O yield single component isotherms. In addition, mixture experiments allow the description and quantification of the interaction of these two adsorbates that has been indicated in literature. Finally, the derived adsorption isotherm is used in a reactor model to assess the intraparticle mass transfer by a comparison of the experimental and predicted transient seen during breakthrough.

In the present work, a series of breakthrough experiments was performed in an adsorption column filled with K-HTC pellets, feeding CO_2 , H_2O , and CO_2 – H_2O mixtures, all in N_2 /Ar, at a reactor temperature of 400 °C and a total pressure of up to 27 bar(a). After integration of the breakthrough curves, adsorption capacities for CO_2 and H_2O were determined and adsorption isotherms were fitted to the data. Subsequently, a reactor model that was previously developed and used for validation of low pressure sorption enhanced reforming [17,18] was updated to simulate the breakthrough experiments.

This paper first presents the experimental procedure and results, yielding an adsorption isotherm that provides a satisfactory description of the measured capacities. Secondly, reactor simulations are used to validate a linear driving force intraparticle model for sorption kinetics.

2. Material and methods

2.1. Experimental procedure

Ideally, mixture adsorption is measured in a dedicated setup that allows for highly accurate measurements (see, for example, the review by [19]. However, for adsorption of CO₂ and H₂O on K-HTC at 400 °C, the standard approach faces particular complications. First of all, it is important to ensure a proper reference state at the start of each experiment. HTC is a double hydroxide, with the general formula $Mg_{(1-x)}Al_x(OH)_2(CO_3)_{(x/2)} \cdot nH_2O$. It has a layered structure and contains hydroxides, carbonates, and water groups. Between 300 and 500 °C, the material goes through several dehydroxylation and decarbonation steps [20,21,14]. The layered structure collapses above approximately 350 °C. Under SEWGS operating conditions, K-HTC is in the middle of a transition to mixed-metal oxide, while still containing carbonate and hydroxide groups, and consequently difficult to fully define. Therefore, in order to insure that the material is always in the same state, a standard regeneration method was used in between the measurements, as described below. Secondly, measuring with a high partial pressure of steam is challenging. At 25 bar partial pressure, H₂O has a dew point of approximately 224 °C, requiring flow control and all parts of the setup to be at least at this temperature in order to prevent condensation and have a stable flow for accurate measurement. Thirdly, sampling and quantifying of various concentrations of H₂O is also not straightforward. One solution to the issues mentioned is to resort to breakthrough experiments to measure the multicomponent isotherm. Hence, breakthrough experiments have been performed at bench scale with MS gas sampling - yielding new insights that are not readily obtained at laboratory scale.

2.1.1. Setup

Experiments were performed in the multicolumn SEWGS test rig, described in detail van Selow et al. by [22]. It comprises

columns of 6 m tall and 38 mm internal diameter. Each column is filled with 4.7×4.7 mm pellets of a potassium-promoted hydrotalcite, produced by Sasol Germany. The hydrotalcite has a Mg/Al ratio of 0.6, and was promoted with approximately 20 wt.% K₂CO₃, as specified by the vendor. During the experiments in the temperature range of 400-450 °C, it is in transition from layered double hydroxide to a mixed-metal oxide. At the time of the breakthrough tests, the pellets had been in the column for more than two years and proven to be stable in various SEWGS cycles for thousands of cycles in total. In order to measure breakthrough of CO₂ and H₂O with an accuracy as high as possible, one of the columns has been adapted for breakthrough measurements by installation of a sample system. The system, shown schematically in Fig. 1, provides two sample lines that connect the setup to a mass spectrometer (MS). The lower line allows the withdrawal of samples of the feed gas and the top line allows extraction of sample gas from the SEWGS column, 2 m downstream the feed connection. A sample flow of approximately 0.5 slpm is drawn from the system, reduced to atmospheric pressure and then mixed with 0.5 slpm of helium, which proved to be sufficiently small to prevent loss of MS signal fidelity yet sufficiently large to prevent problems with condensation. The sample flow is then fed to the MS at 80 °C, measuring the responses for Ar, H_2O , CO_2 , and N_2 .

2.1.2. Breakthrough experiments

In order to measure the uptake of CO_2 and H_2O separately, the sorbent was cleaned and dried in a number of steps. (1) Initially, the sorbent was saturated with steam at 400 °C and 27 bar(a), purging any remaining CO_2 from the material. (2) The purge was repeated at 450 °C, further removing CO_2 that remained on the sorbent. (3) The sorbent was dried with N_2 at 450 °C and 4 bar(a) pressure, until no H_2O was measured in the column outlet gas, followed by cooling to 400 °C in dry N_2 .

The $\rm H_2O$ breakthrough capacity was measured at three levels of total pressure: 8, 17.5, and 27 bar(a). At each pressure level, breakthrough measurements with 11, 43, and 78 vol.% $\rm H_2O$ in $\rm Ar/N_2$ were performed sequentially. In order to minimise the number of regeneration steps, both the second and third concentration levels were measured relative to the first concentration level. Accordingly, 11% $\rm H_2O$ was measured first, followed directly by measurement of the additional capacity at 43%. Afterwards, the sorbent in the column was saturated with steam and then dried with $\rm N_2$, followed by re-equilibration with 11% $\rm H_2O$. Then, the final point at 78% $\rm H_2O$ was measured, again relative to the uptake at 11%. In

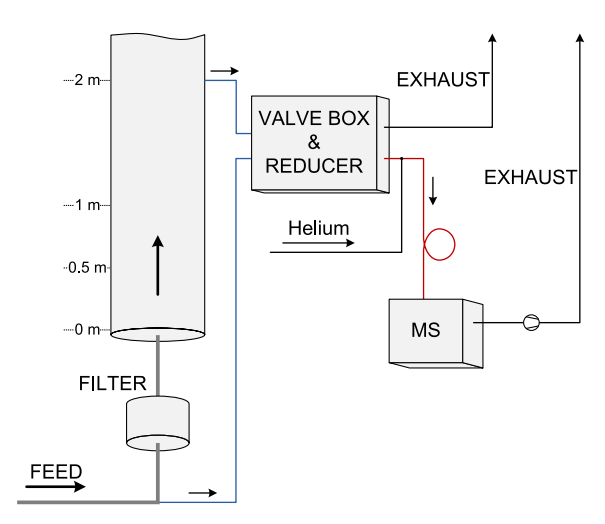


Fig. 1. Bottom part of SEWGS column and installed sample system.

between the pressure levels and before measuring 11% H₂O, the sorbent was dried at 450 °C and cooled back to 400 °C in N₂.

Upon completion of the H_2O breakthrough measurements, pure CO_2 breakthrough experiments were performed. These were carried out at 7, 12, 17, 22, and 27 bar(a) total pressure. In between the pressure levels, the sorbent was purged with steam at 27 bar(a) and dried in N_2 at 4 bar(a). At each pressure setting, measurements were performed with 3% CO_2 directly followed by 33% and 71% CO_2 in Ar/N_2 , measuring the additional uptake after the preceding concentration.

The CO2-H2O breakthrough experiments were aimed at measuring excess adsorption of CO₂ and H₂O at 400 °C and 27 bar(a). To this end, the column was operated in cyclic mode, each breakthrough experiment being preceded by a sequence of preconditioning steps: (1) saturation of the column with 18.5 vol.% CO₂ and 37.0 vol.% H₂O in N₂ at 27 bar(a) total pressure, (2) depressurisation to atmospheric pressure. (3) purge by H₂O until no more CO₂ came off followed by switching off the purge gas to depressurise the column to atmospheric pressure again, and (4) repressurization of the column to 27 bar(a) with dry N2. Thus, the column is as much as possible in the same state at the start of each breakthrough experiment, containing 1 bar H₂O in N₂. By design of experiments, 32 conditions had been defined (that were all measured twice in randomised order except for the centre point which was measure nine times throughout the experimental programme), with CO₂ partial pressures in the range of 0.5-24 bar and H₂O partial pressures in the range of 4-24 bar, all with Ar tracer and balance N₂ at 27 bar(a) total pressure. The Ar tracer serves to describe the hydrodynamic characteristics of the column and sampling system.

2.1.3. Regeneration experiments

For the purpose of evaluating the kinetics of regeneration of the adsorbent, a series of regeneration experiments has been carried out. In these experiments, the column was saturated with 17 vol.% $\rm CO_2$ and 25 vol.% $\rm H_2O$ in $\rm N_2$ at 27 bar(a) and 400 °C. Then, a counter current rinse was performed with 30 slpm steam, followed by depressurisation to atmospheric pressure, and purge with 18 slpm steam. During these steps, the dry outlet flow rate was measured after the gas cooling and condensate removal. The same experiment was also carried out with 38 slpm purge flow rate.

2.2. Data interpretation and model development

2.2.1. Equilibrium data from breakthrough experiments

Setting up a material balance for component i over the column, accumulation of component i between t=0 and complete breakthrough $(t=t_e)$ must equal the difference between the molar inflow and outflow rates, i.e.

$$\frac{y_{i}(t_{e})p}{RT}V_{g} + q_{i}(t_{e})m_{s} - \frac{y_{i}(0)p}{RT}V_{g} - q_{i}(0)m_{s}
= t_{e}F_{i,in} - \int_{0}^{t_{e}} (y_{i}F)_{out}dt$$
(3)

The trapezoidal rule has been used for approximating the integral by a summation over discrete measurement data. Prior to breakthrough of CO_2 and $\mathrm{H}_2\mathrm{O}$, the breakthrough of Ar (assuming $q_{Ar}=0$) is integrated to obtain V_g , the total interparticle and intraparticle gas volume in the column. After breakthrough, the Ar signal is used for quantifying the outlet flow rate prior to and during breakthrough of $\mathrm{H}_2\mathrm{O}$ and CO_2 . Eq. (3) can then be used to compute q_{CO_2} and $q_{\mathrm{H}_2\mathrm{O}}$.

2.2.2. Adsorption isotherm

Adsorption isotherms are derived on the basis of the underlying physics of sorbent-sorbate interactions. As presented in the Introduction, the main body of literature is based on Langmuir and Freundlich isotherms. These are derived from adsorption on specific surface sites. Indeed, Walspurger et al. [23] suggested that a transformation occurs of potassium carbonate at the surface of HTC and that aluminium oxide - potassium carbonate interaction creates the strongly basic active sites for CO₂ adsorption. This, however, is not to say that the surface sites on K-HTC are homogeneous, nor that each site can adsorb only a single molecule. In fact, many authors have proposed multi-site adsorption models for lower partial pressures and the sorbates may interact as well, see e.g. [24.8.25–28] and the discussion in Section 3.2. The current work. however, focuses on higher partial pressures and both the data set and the experimental equipment does not allow to discern multi-site or multi-component interaction mechanisms at low partial pressures. In addition to surface sites, nanopores may play an important role at higher pressures. Soares et al. [29] and later Maroño et al. [30] measured a significant volume of nanopores that may additionally contribute to the adsorption capacity for CO₂. Nanopore adsorption occurs above a certain partial pressure threshold when surface adsorption turns into pore volume filling [31]. For H₂O, little is known about adsorption on K-HTC. van Selow et al. [16] have proposed a Langmuir isotherm. On several clays, however, Hatch et al. [32] recently measured the contribution of surface and nanopores for the adsorption of H₂O.

A model is derived here that is based on contributions of surface and nanopores for the adsorption of CO_2 and H_2O . Whereas the surface sites are specific in the sense that they adsorb either CO_2 or H_2O , competitive adsorption is expected in the nanopores. Surface adsorption of CO_2 is described by a Langmuir isotherm, concurring with most studies in literature. For H_2O , a Freundlich isotherm is used for the surface contribution, reflecting the presumed heterogeneous character of the sites for H_2O . Given the range of measurement and within the range of uncertainty, the choice is arbitrary. The nanopore contribution is described using a Dubinin–Astakhov equation based on volume filling theory. In such a case, assuming no lateral interactions between adsorbed species, the amount of gas adsorbed is determined by the limiting nanopore volume V_0 , pore-size distribution parameter m, and the nanopore-sorbate interaction energy E [33,34,31]. Thus, for CO_2 ,

$$q_{\text{CO}_2}^{\text{eq}} = \frac{q_{\text{CO}_2}^s K_{\text{CO}_2} p_{\text{CO}_2}}{1 + K_{\text{CO}_2} p_{\text{CO}_2}} + \frac{A_{\text{CO}_2} (V_0 - V_0 A_{\text{H}_2\text{O}})}{\nu_{\text{m,CO}_2} (1 - A_{\text{CO}_2} A_{\text{H}_2\text{O}})}$$
(4)

and for H₂O,

$$q_{\rm H_2O}^{\rm eq} = K_{\rm H_2O} p_{\rm H_2O}^{1/n} + \frac{A_{\rm H_2O} (V_0 - V_0 A_{\rm CO_2})}{\nu_{m,\rm H_2O} (1 - A_{\rm CO}, A_{\rm H_2O})} \tag{5}$$

with

$$A_{i} = \exp\left(-\left[\left(\frac{RT}{E_{i}}\right)\ln\left(\frac{p_{0,i}}{p_{i}}\right)\right]^{m_{i}}\right) \tag{6}$$

$$p_{0,i} = p_{c,i} \left(\frac{T}{T_{c,i}}\right)^2 \tag{7}$$

$$\nu_{m,i} = \frac{RT_{c,i}}{8p_{c,i}} \left(\frac{T}{T_{c,i}}\right)^{0.6} \tag{8}$$

2.2.3. Intraparticle mass transfer resistance

In order to assess the kinetics of adsorption, that is the intraparticle mass transfer resistance and the resulting width of the mass transfer zone, a reactor model was developed, based on a previous reactor model for low pressure sorption enhanced reforming [17,18]. The transport equations solved are shown in Table 1,

Table 1 Reactor model equations.

Continuity	$rac{\partial ho}{\partial t} = -rac{\partial ho v}{\partial z} + rac{1-\epsilon_b}{\epsilon_b} a_p \sum_i M_i N_i$	A
Momentum	$0 = -\frac{\partial p}{\partial \tau} - f \frac{\rho u u}{du}$	В
Heat balance	$\left(\epsilon_b \rho C_p + (1 - \epsilon_b) \rho_p C_{p,p}\right) \frac{\partial T}{\partial t} = -\rho C_p u \frac{\partial T}{\partial z} + \frac{\partial}{\partial z} \left(\lambda \frac{\partial T}{\partial z}\right) + \frac{4U(T_w - T)}{d_r} - (1 - \epsilon_b) \rho_p \left((-\Delta H_r) r_{\text{WGS}} + \sum_i (-\Delta H_{a,i} \frac{d(q_i)}{dt})\right)$	C
Mass balance	$rac{\partial (ho\omega_i)}{\partial t} = -rac{\partial ho v\omega_i}{\partial z} + rac{\partial}{\partial z} \left(D_2 ho rac{\partial \omega_i}{\partial z}\right) + rac{1-\epsilon_b}{\epsilon_b} a_p M_i N_i$	D
State	$pM_{\omega} = \rho RT$	E
	$M_{\omega} = \left(\sum_i rac{\omega_i}{M_i} ight)^{-1}$	F

Table 2 Intraparticle equations.

Intraparticle mass balance	$\frac{d\langle c_i \rangle}{dt} = k_{\mathrm{LDF},i} (c_{\mathrm{int},i} - \langle c_i \rangle)$	G
LDF mass transfer coefficient	$k_{ ext{LDF},i} = rac{15\mathcal{D}_{p,i}}{r_p^2(\epsilon_p + ho_prac{\partial q_i}{\partial c_i})}$	Н
Multicomponent isotherm	$\langle q_i \rangle = f(\langle c_{1N} \rangle)$	I

Table 3 SEWGS process parameters.

I.	2	m (breakthrough)
L		, , ,
	6	m (regeneration)
d_r	38	mm
d_p	4.4	mm
$ ho_p$	1074	$ m kg~m^{-3}$
ϵ_b	0.4	
ϵ_p	0.3	
T_{wall}	400	°C
p	27	bar (breakthrough)
$u_{\rm feed}$	0.029	${ m m\ s^{-1}}$

now including accurate description of transport of concentrated species and density changes. The feed flow rate is specified at the column inlet, the pressure at the column outlet. Danckwerts boundary conditions are used for the heat and mass balances. Using the method of lines, the equations are discretised on a uniform grid in the axial direction with a Barton flux delimited second order upwind scheme for the convective terms, second order implicit central differencing for the dispersion terms, and semiimplicit linearised source terms. The resulting time-dependent ordinary differential equations are integrated in time with first order Euler scheme with time step adaptation. The equations for the intraparticle model are shown in Table 2. They are derived from the common linear driving force assumption [35], for porous spherical particles. The adsorption isotherm (G) has been derived in Section 2.2.2. Constitutive equations have been taken from literature [36,35,37–39]. Model parameters are shown in Table 3.

3. Results and discussion

3.1. Breakthrough capacities for CO₂, H₂O, and mixtures thereof

Adsorption capacities for CO_2 and H_2O have been derived from the breakthrough measurements. The data points in Figs. 2 and 3 show the pure component capacities (note that all lines are drawn with the isotherm as derived in Section 3.2 from the full data set, including mixture data), the data points in Fig. 4 show the mixture capacities. The pure component capacities in Fig. 2 for CO_2 follow a two-step adsorption mechanism, of which the first contribution up to 0.4 mol kg^{-1} is attributed to surface sites and the additional adsorption at partial pressures of 3 bar and over corresponds to nanopore adsorption. Given the current range of measurements, it is not possible to discern a more detailed interaction at the lower

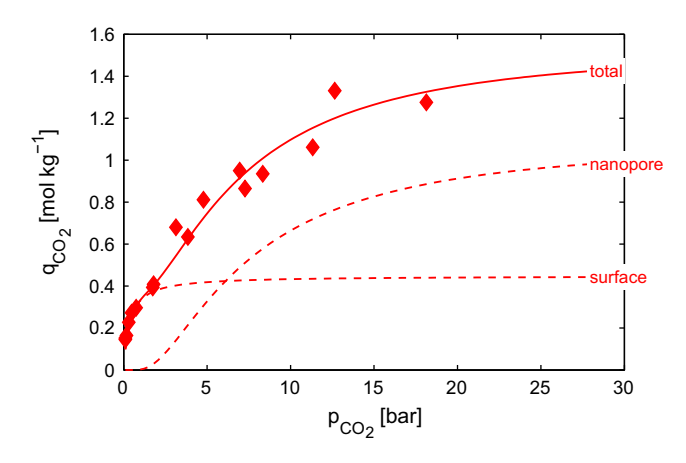


Fig. 2. Pure CO_2 breakthrough capacities versus CO_2 partial pressure (diamonds), predicted capacity (line), contribution of different sites (dashed lines).

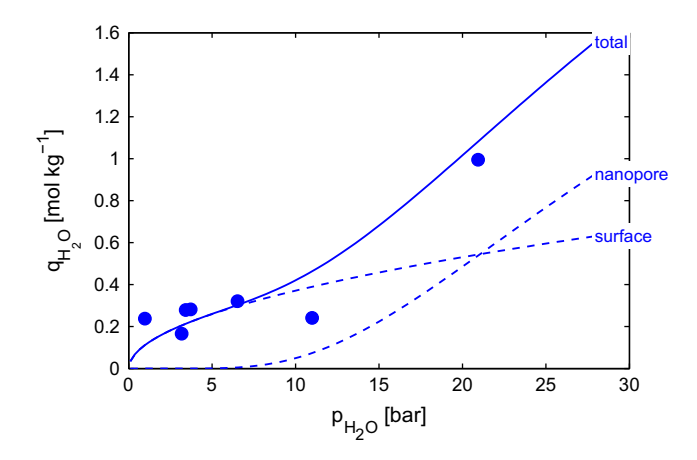


Fig. 3. Pure H_2O breakthrough capacities versus H_2O partial pressure (circles), predicted capacity (line), contribution of different sites (dashed lines).

concentration levels, as for example presented by Lee et al. [8]. For H_2O , similar trends result. Up until 12 bar partial pressure, the measured capacites for H_2O show a levelling off of the surface contribution around 0.3 mol kg $^{-1}$, which is in line with the Langmuir isotherm proposed by van Selow et al. [16]. Noticeably, however, the single datapoint above 20 bar suggests an additional nanopore adsorption mechanism. Over the full partial pressure range, the trend in H_2O adsorption data is similar to the trend observed by Hatch et al. [32], and supports the hypothesis of a binary mechanism.

3.2. Adsorption isotherm

The entire experimental data set was used to fit a multicomponent adsorption isotherm for the system. A good fit was obtained

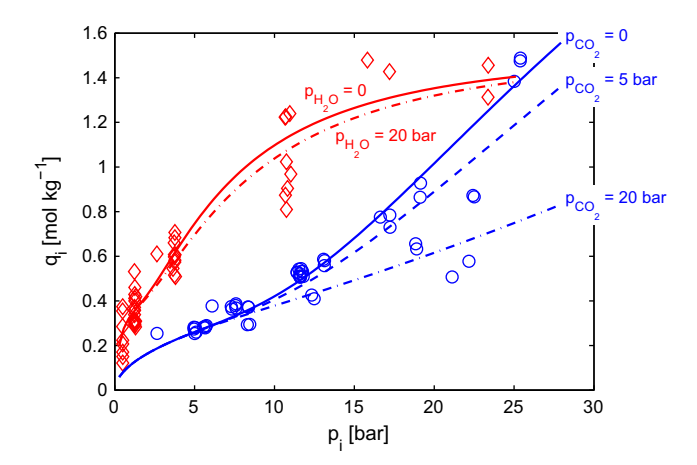


Fig. 4. CO_2-H_2O mixture breakthrough capacities for CO_2 (red, open diamonds) and H_2O (blue, open circles, corrected for the predicted remaining amount of H_2O adsorbed after regeneration) versus partial pressure, predicted pure component capacities (line) and mixture capacities (dashed lines). (For interpretation of the references to colour in this figure legend, the reader is referred to the web version of this article.)

with two double isotherms, consisting of a surface and nanopore contribution (Eqs. (4)–(8)). The regressed parameters and statistics are shown in Table 4. The isotherms are added to Figs. 2–4 for easy comparison. Parity plots of the predicted versus measured adsorption capacity, both for the single components and mixtures, are shown in Figs. 5 and 6.

Obtaining data with high accuracy from a bench scale setup as the one used in this study presents a challenge and consequently there is significant scatter in the data, especially in the mixture data, and the number of data points for low concentrations is small. In this respect, the use of alternative experimental techniques could pave the way for modelling of the low pressure interaction. Tapered element oscillating microbalance experiments have been successfully employed to measure the thermal composition of hydrotalcites at temperatures up to 700 °C [40], to measure equilibria and kinetics of n-hexane and n-heptane adsorption on catalyst particles [41], and to study the effect of steam upon CO₂ capture by several high-temperature sorbents at sorption-enhanced steam methane reforming conditions [42]. Alternatively, full binary equilibrium characterisation could be performed by equilibrating the solid under flow conditions followed by complete desorption and characterisation of total column contents, or by a combination of gravimetric and volumetric techniques [19]. Still, the current set of experiments provides values that would be very difficult to measure otherwise. The scatter gives rise to relatively large confidence intervals in the parameter estimates and the small number of data points in the low

Table 4 Regressed multicomponent isotherm parameters (Eqs. (4)–(8)) confidence interval.

Parameter	Estimate	
$q_{\mathrm{CO}_2}^s$	0.45 ± 0.13	mol kg ⁻¹
K_{CO_2}	28 ± 26	MPa^{-1}
E_{CO_2}	23 ± 1	kJ mol ⁻¹
$m_{{\rm CO}_2}$	5.2 ± 1.5	-
$K_{\text{H}_2\text{O}}$	0.37 ± 0.07	$\mathrm{mol}\ \mathrm{kg}^{-1}\ \mathrm{MPa}^{-1/n}$
n	1.9 ± 0.5	
$E_{\rm H_2O}$	12 ± 1	kJ mol ⁻¹
$m_{\rm H_2O}$	3.6 ± 0.8	-
V_0	74 ± 17	$cm^3 kg^{-1}$

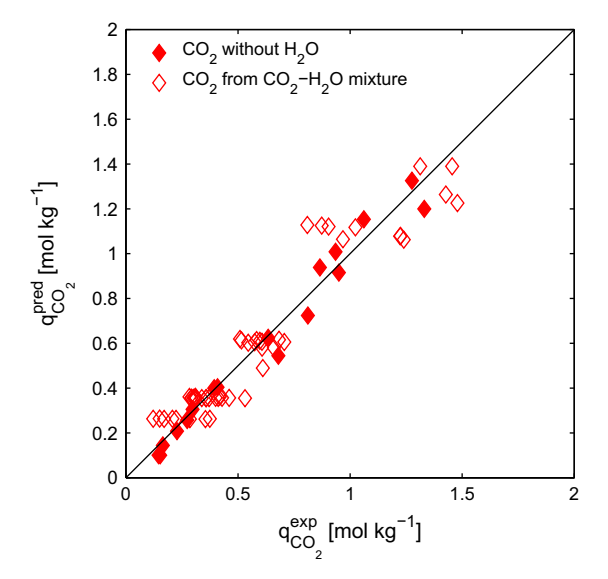


Fig. 5. Parity plot of predicted CO₂ capacities versus measured CO₂ capacities.

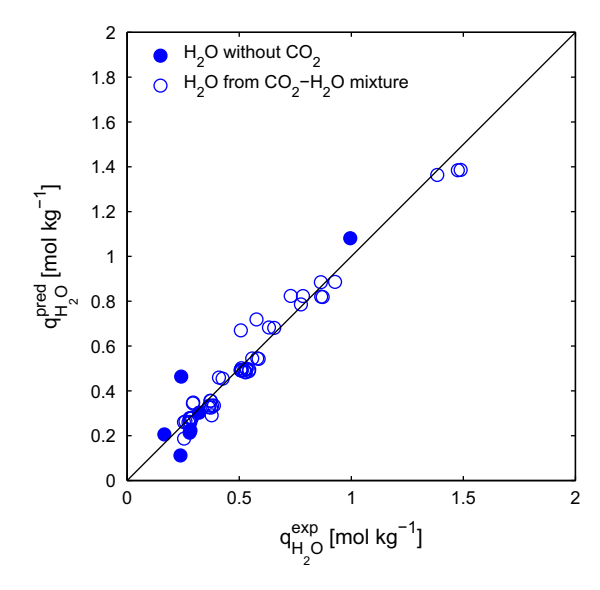


Fig. 6. Parity plot of predicted H₂O capacities versus measured H₂O capacities.

concentration region further adds to the uncertainty for surface adsorption parameters, particularly K_{CO_2} (see Table 4). Nevertheless, all model parameter estimates are statistically significant at 90% confidence interval. The match of the model with less scattered single component data, Figs. 2 and 3, is good. The trends observed in the parity plot for CO_2 (Fig. 5) are randomly scattered in time and with H_2O concentration and reflect the accuracy of measurement for $\text{CO}_2\text{-H}_2\text{O}$ mixtures. The absence of trends for the pure CO_2 data plot for H_2O (Fig. 6) gives further confidence to the assumptions made in deriving the adsorption model.

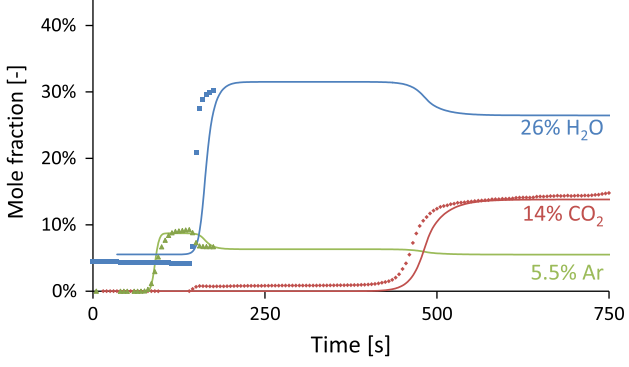
Within the range of uncertainties, the values determined here are in agreement with values published by other groups. For adsorption of CO_2 on K-HTC, Lee et al. [8, Table 3] reports monolayer capacities in the range of 0.25–0.45 mol kg $^{-1}$ (compared to $q_{CO_2}^s = 0.45$ mol kg $^{-1}$ in this work) yet much higher gas–solid interaction parameters at 400 °C in the range of 167–369 MPa $^{-1}$. The difference might be due to the uncertainty in the Langmuir parameters but could also be caused by differences in surface characteristics of the sorbent. In a study with limited data at lower partial

pressures [28] report 44.5 MPa⁻¹, which is larger than yet within the confidence interval of the present result. For H_2O literature data is scarce. Still the Freundlich exponent n=1.9, that quantifies the nonlinearity of the isotherm, is in the range of 1.7–5.1 reported for the adsorption of H_2O on various clays [32]. For the nanopore adsorption model, few relevant studies are available. The nanopore volume in the current work is estimated at 74 cm³ kg⁻¹, while [29] has reported 73.3 cm³ kg⁻¹ for MG30 and Maroño et al. [30] found similar pore volumes in the range of 50–60 cm³ kg⁻¹ for KMG30, depending on the temperature of calcination. The parameter m (5.2 for CO_2 , 3.6 for H_2O) characterises nanopore heterogeneity, where values generally vary between 1 and 6 [31]. The characteristic energies E (Table 4: $E_{CO_2}/RT = 4.1$, and $E_{H_2O}/RT = 2.1$) are typical values for nanopore-sorbate interaction energies using the Dubinin–Astakhov model [34,31].

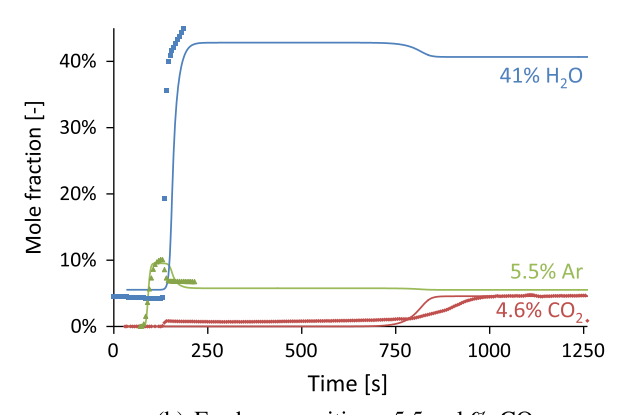
The trends in the adsorption of CO₂ and H₂O on K-HTC observed here have been reported by other authors as well, although there are important differences that arise mainly because of the difference in partial pressures of the adsorbates. In contrast with the present model, the capacity for CO₂ has been reported to increase for low partial pressures of steam, compared to dry conditions [7,24,43,25]. The presence of steam has been suggested to create adsorption sites through the formation of hydroxides, which in turn activate adsorption sites [7], form bicarbonates [25] or carbonates [26] in the presence of CO₂. At lower partial pressures, steam will probably enhance the adsorption of CO₂ in the present system as well, but the smallest steam partial pressure in these experiments was 4 bar and the set of experimental data thus does not allow to discern these interactions. Again, additional experimental work, such as Fourier transform infrared spectroscopy, might prove useful in elucidating the low partial pressure mechanisms in more detail [25]. At higher steam partial pressures, however, competitive adsorption has been observed [28]. For CO₂ adsorption itself, a number of different mechanisms has been suggested to contribute to the adsorption capacity. Ebner et al. [12], Oliveira et al. [9] and Wu et al. [13] have all suggested a combination of physisorption and chemisorption for CO₂. [8] observed a binary mechanism up to 3 bar CO₂ partial pressure, suggesting a mechanism of chemisorption and surface complexation. Based on experiments with 1 bar CO₂, [27] found physical and chemical contributions to the adsorption capacity and concluded that not only the surface, but also morphology and pore structure are essential to achieve a high adsorption capacity. The present work has produced little data in the low pressure range that was studied by these authors. However, it should be noted that high pressure H₂O is able to desorb traces of CO₂ that remain on the sorbent after low pressure regeneration, as shown in Fig. 7, after breakthrough of H₂O and before CO₂ breakthrough. This is indeed an indication of interaction between high pressure H₂O and small amounts of CO₂ adsorbed. Therefore, it seems probable that the surface contribution for CO₂ in Eq. (4), and possibly for H₂O in Eq. (5), is the sum of contributions from several different mechanisms where interaction may also play a role. Additionally, the present work reaffirms the importance of the nanostructure of the sorbent, predominantly at higher partial pressures. In this respect, a clear indicator is the observation that the impact of CO₂ on the capacity for H₂O is much stronger than vice versa. This can hardly be explained by a site-specific model but is well accounted for by the nanopore model (cf. Fig. 4). The larger molar volume of CO₂ ($\nu_{m,\text{CO}_2} = 69 \text{ cm}^3 \text{ mol}^{-1}$) compared to H₂O ($\nu_{m,\text{H}_2\text{O}} = 31 \text{ cm}^3 \text{ mol}^{-1}$) ensures that the available nanopore volume is more strongly attenuated by CO₂ than by H₂O.

3.3. Kinetics of adsorption and desorption

The heterogeneous linear driving force relation used in this work is based on the intraparticle concentrations (Equation G,



(a) Feed composition: 14 vol.% CO_2 , 26 vol.% H_2O , 5.5 vol.% Ar, balance N_2



(b) Feed composition: 5.5 vol.% CO₂, 41 vol.% H₂O, 4.6 vol.% Ar, balance N₂

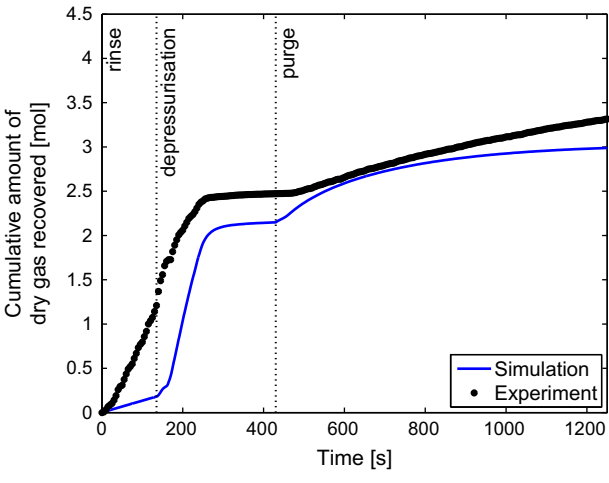
Fig. 7. Predicted (lines) and measured (symbols) breakthrough of Ar, $\rm H_2O$, and $\rm CO_2$ at 400 °C, 27 bar(a) and different feed compositions.

Table 2). A similar relation has been used by [13]. The equation accounts for contributions of intraparticle gas phase (through $c_{\text{int},i}$) as well as intraparticle surface and nanopore accumulation terms (through q_i). It approximates the rigorous intraparticle diffusion equations to a numerically efficient ordinary differential equation, an approach which is common practice in PSA modelling [38]. The heterogeneous linear driving force relation is different from the homogeneous relation that has been used earlier [7,8]:

$$\frac{d\langle q_i \rangle}{dt} = k'_{\text{LDF},i} \left(q_i^{\text{eq}} - \langle q_i \rangle \right) \tag{9}$$

The latter equation derives from Equation G (Table 2) [44], but only when the isotherm equation can be rewritten into a form that explicitly expresses $c_{\text{int},i}$ as a function of q_i^{eq} . As this is not the case for the current isotherm (Eqs. (4) and (5)), the homogeneous LDF cannot be used to describe the experimental observations of the kinetics for both adsorption and regeneration in the present work.

The heterogeneous linear driving force relation only approximates intraparticle resistances to mass transfer. It can be expanded or elaborated in more detail by accounting for the resistance in the crystals, or multicomponent mass transfer. Wu et al. [13], for example, use a double linear driving force approach. However, such an approach does not seem to be justified in the present study, unless the internal structure of the particles were to be characterised with much more detailed information on the particle morphology. Besides, the match between experiment and model is fair, as shown in Figs. 7 and 8. During breakthrough, as shown in Fig. 7, the stoichiometric breakthrough time of each of the



(a) Purge flow rate 0.87 kg/h H₂O

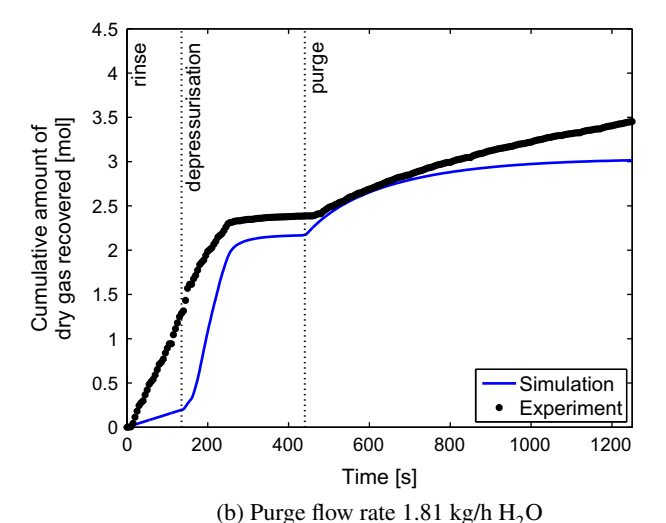


Fig. 8. Desorption curves for rinse, depressurisation and purge with varying purge flow rate.

species is predicted well. This indicates that the sorption capacity for these conditions is accurately predicted by the proposed multicomponent isotherm. The transient of breakthrough is also represented well by the model, except for CO_2 in case (b) with 4.6 vol.% CO_2 in the feed, where the transient is somewhat faster in the model than in the measurement. In this context, however, it should be noted that measurements with CO_2 – H_2O mixtures at these low CO_2 concentrations are non-trivial in the current setup. A fact that also shows in the relatively large scatter for the data points for CO_2 partial pressures below 2 bar (Fig. 4). For the desorption experiments shown in Fig. 8, the model predicts a slower desorption of CO_2 than measured experimentally. Apart from a difference in absolute amount of CO_2 adsorbed, this may be at least partly caused by pressure dynamics in the bench scale system that are not fully represented in the model.

4. Conclusion

Breakthrough experiments with CO_2 , H_2O , and mixtures thereof on a SEWGS bench scale unit have yielded the capacity and kinetics of adsorption on K-HTC over a wide range of partial pressures, up to $24 \, \text{bar}(a)$ and at $400 \, ^{\circ}\text{C}$ that have not been reported before. Capacities of up to $1.5 \, \text{mol kg}^{-1}$ have been measured, both for CO_2 and for H_2O . This data set has been successfully used to fit a

multicomponent adsorption isotherm. The isotherm consists of a lower partial pressure part where surface adsorption dominates and a high partial pressure nanopore adsorption part. Surface adsorption occurs at specific sites for CO_2 or H_2O . In contrast, the nanopore adsorption mechanism is competitive and explains the interaction observed in the capacity data at partial pressures over 5 bar.

A SEWGS reactor model has been developed. The model uses a heterogeneous linear driving force approximation for the intraparticle mass transfer resistance, reflecting the porous character of the particle. Isotherm and linear driving force approximation, incorporated into the reactor model, can predict well both the breakthrough and the regeneration behaviour during SEWGS experiments. The model provides important information on the competitive adsorption of CO₂ and H₂O in a SEWGS cycle.

Acknowledgements

Dr. Stéphane Walspurger of ECN Sustainable Process Technology is kindly acknowledged for fruitful discussions. This research has been carried out in the context of the CATO-2 programme. CATO-2 is the Dutch national research programme on CO₂ Capture and Storage technology (CCS). The programme is financially supported by the Dutch government (Ministry of Economic Affairs) and the CATO-2 consortium parties.

Appendix A. Supplementary material

Supplementary data associated with this article can be found, in the online version, at http://dx.doi.org/10.1016/j.cej.2014.03.056.

References

- J.R. Hufton, S. Mayorga, S. Sircar, Sorption-enhanced reaction process for hydrogen production, AIChE J. 45 (1999) 248–256.
- [2] Z. Yong, V. Mata, A.E. Rodrigues, Adsorption of carbon dioxide at high temperature – a review, Sep. Purif. Technol. 26 (2002) 195–205.
- [3] K.B. Lee, M.G. Beaver, H.S. Caram, S. Sircar, Reversible chemisorbents for carbon dioxide and their potential applications, Ind. Eng. Chem. Res. 47 (2008) 8048–8062
- [4] E.R. van Selow, P.D. Cobden, P.A. Verbraeken, J.R. Hufton, R.W. van Den Brink, Carbon capture by sorption-enhanced water-gas shift reaction process using hydrotalcite-based material, Ind. Eng. Chem. Res. 48 (2009) 4184–4193.
- [5] G. Manzolini, E. Macchi, M. Gazzani, CO₂ capture in natural gas combined cycle with SEWGS. Part B: Economic assessment, Int. J. Greenhouse Gas Control 12 (2013) 502–509.
- [6] G. Manzolini, E. Macchi, M. Gazzani, CO₂ capture in integrated gasification combined cycle with SEWGS – Part B: Economic assessment, Fuel 105 (2013) 220–227.
- [7] Y. Ding, E. Alpay, Equilibria and kinetics of CO₂ adsorption on hydrotalcite adsorbent, Chem. Eng. Sci. 55 (2000) 3461–3474.
- [8] K.B. Lee, A. Verdooren, H.S. Caram, S. Sircar, Chemisorption of carbon dioxide on potassium-carbonate-promoted hydrotalcite, J. Colloid Interf. Sci. 308 (2007) 30–39.
- [9] E.L.G. Oliveira, C.A. Grande, A.E. Rodrigues, CO₂ sorption on hydrotalcite and alkali-modified (K and Cs) hydrotalcites at high temperatures, Sep. Purif. Technol. 62 (2008) 137–147.
- [10] M.H. Halabi, M.H.J.M. de Croon, J. van der Schaaf, P.D. Cobden, J.C. Schouten, High capacity potassium-promoted hydrotalcite for CO₂ capture in H₂ production, Int. J. Hydrogen Energy 37 (2012) 4516–4525.
- [11] A.D. Ebner, S.P. Reynolds, J.A. Ritter, Understanding the adsorption and desorption behavior of CO₂ on a K-promoted hydrotalcite-like compound (htlc) through nonequilibrium dynamic isotherms, Ind. Eng. Chem. Res. 45 (2006) 6387-6392.
- [12] A.D. Ebner, S.P. Reynolds, J.A. Ritter, Nonequilibrium kinetic model that describes the reversible adsorption and desorption behavior of CO₂ in a Kpromoted hydrotalcite-like compound, Ind. Eng. Chem. Res. 46 (2007) 1737– 1744
- [13] Y.-J. Wu, P. Li, J.-G. Yu, A.F. Cunha, A.E. Rodrigues, K-promoted hydrotalcites for CO₂ capture in sorption enhanced reactions, Chem. Eng. Technol. 36 (2013) 567–574
- [14] S. Walspurger, P.D. Cobden, O.V. Safonova, Y. Wu, E.J. Anthony, High CO₂ storage capacity in alkali-promoted hydrotalcite-based material: in situ detection of reversible formation of magnesium carbonate, Chem. Euro. J. 16 (2010) 12694–12700.

- [15] M. Maroño, Y. Torreiro, L. Gutierrez, Influence of steam partial pressures in the CO₂ capture capacity of K-doped hydrotalcite-based sorbents for their application to SEWGS processes, Int. J. Greenhouse Gas Control 14 (2013) 183–192
- [16] E.R. van Selow, P.D. Cobden, R.W. van den Brink, A. Wright, V. White, P. Hinderink, J.R. Hufton, Carbon Dioxide Capture for Storage in Deep Geologic Formations, Berks, CPL Press, 2009.
- [17] H.T.J. Reijers, J. Boon, G.D. Elzinga, P.D. Cobden, W.G. Haije, R.W. van den Brink, Modeling study of the sorption-enhanced reaction process for CO₂ capture. I. Model development and validation, Ind. Eng. Chem. Res. 48 (2009) 6966–6974.
- [18] H.T.J. Reijers, J. Boon, G.D. Elzinga, P.D. Cobden, W.G. Haije, R.W. van den Brink, Modeling study of the sorption-enhanced reaction process for CO₂ capture. II. Application to steam-methane reforming, Ind. Eng. Chem. Res. 48 (2009) 6975–6982.
- [19] O. Talu, Measurement and analysis of mixture adsorption equilibrium in porous solids, Chem.-Ing.-Tech. 83 (2011) 67–82.
- [20] W.T. Reichle, S.Y. Kang, D.S. Everhardt, The nature of the thermal decomposition of a catalytically active anionic clay mineral, J. Catal. 101 (1986) 352–359.
- [21] F. Cavani, F. Trifirò, A. Vaccari, Hydrotalcite-type anionic clays: preparation, properties and applications, Catal. Today 11 (1991) 173–301.
- [22] E.R. van Selow, P.D. Cobden, R.W. van den Brink, J.R. Hufton, A. Wright, Performance of sorption-enhanced water-gas shift as a pre-combustion CO₂ capture technology, Energy Proc. 1 (2009) 689–696.
- [23] S. Walspurger, L. Boels, P.D. Cobden, G.D. Elzinga, W.G. Haije, R.W. van den Brink, The crucial role of the K*-aluminium oxide interaction in K*-promoted alumina- and hydrotalcite-based materials for CO₂ sorption at high temperatures, ChemSusChem 1 (2008) 643–650.
- [24] Z. Yong, V. Mata, A.E. Rodrigues, Adsorption of carbon dioxide onto hydrotalcite-like compounds (HTlcs) at high temperatures, Ind. Eng. Chem. Res. 40 (2001) 204–209.
- [25] M.K. Ram Reddy, Z.P. Xu, G.Q. Lu, J.C. Diniz da Costa, Influence of water on high-temperature CO₂ capture using layered double hydroxide derivatives, Ind. Eng. Chem. Res. 47 (2008) 2630–2635.
- [26] S. Walspurger, S. de Munck, P.D. Cobden, W.G. Haije, R.W. van den Brink, O.V. Safonova, Correlation between structural rearrangement of hydrotalcite-type materials and CO₂ sorption processes under pre-combustion decarbonisation conditions, Energy Proc. 4 (2011) 1162–1167. 10th International Conference on Greenhouse Gas Control Technologies.
- [27] Q. Wang, H.H. Tay, Z. Guo, L. Chen, Y. Liu, J. Chang, Z. Zhong, J. Luo, A. Borgna, Morphology and composition controllable synthesis of Mg–Al–CO₃ hydrotalcites by tuning the synthesis pH and the CO₂ capture capacity, Appl. Clay Sci. 55 (2012) 18–26.
- [28] E.R. van Selow, P.D. Cobden, H.A.J. van Dijk, S. Walspurger, P.A. Verbraeken, D. Jansen, Qualification of the ALKASORB sorbent for the sorption-enhanced water-gas shift process, Energy Proc. 37 (2013) 180-189. GHGT-11.

- [29] J.L. Soares, R.F.P.M. Moreira, H.J. José, C.A. Grande, A.E. Rodrigues, Hydrotalcite materials for carbon dioxide adsorption at high temperatures: characterization and diffusivity measurements, Separ. Sci. Technol. 39 (2005) 1989–2010.
- [30] M. Maroño, Y. Torreiro, L. Montenegro, J. Sánchez, Lab-scale tests of different materials for the selection of suitable sorbents for CO₂ capture with H₂ production in IGCC processes, Fuel 116 (2014) 861–870.
- [31] D.D. Do, Adsorption Analysis: Equilibria and Kinetics, Imperial College Press, 1998
- [32] C. Hatch, J.S. Wiese, C.C. Crane, K.J. Harris, H.G. Kloss, J. Baltrusaitis, Water adsorption on clay minerals as a function of relative humidity: application of BET and Freundlich adsorption models, Langmuir 28 (2012) 1790–1803.
- [33] S. Ozawa, S. Kusumi, Y. Ogino, Physical adsorption of gases at high pressure. IV. An improvement of the Dubinin-Astakhov adsorption equation, J. Colloid Interface Sci. 56 (1976) 83–91.
- [34] S.J. Doong, R.T. Yang, A simple potential-theory model for predicting mixed-gas adsorption, Ind. Eng. Chem. Res. 27 (1988) 630–635.
- [35] D.M. Ruthven, Principles of Adsorption and Adsorption Processes, Wiley-Interscience, New York, 1984.
- [36] R.B. Bird, W.E. Stewart, E.N. Lightfoot, Transport Phenomena, Wiley, New York, 1960
- [37] K.R. Westerterp, W.P.M. van Swaaij, A.A.C.M. Beenackers, Chemical Reactor Design and Operation, second ed., Wiley, Chichester, 1987.
- [38] R.T. Yang, Gas Separation by Adsorption Processes, Imperial College Press, 1987.
- [39] B.E. Poling, J.M. Prausnitz, J.P. O'Connell, The Properties of Gases and Liquids, fifth ed., McGraw-Hill, 2001.
- [40] J. Pérez-Ramírez, S. Abelló, Thermal decomposition of hydrotalcite-like compounds studied by a novel tapered element oscillating microbalance (TEOM): comparison with TGA and DTA, Thermochim. Acta 444 (2006) 75–82.
- [41] E. Alpay, D. Chadwick, L.S. Kershenbaum, P.J. Barrie, C. Sivadinarayana, L.F. Gladden, TEOM analysis of the equilibria and kinetics of n-hexane and n-heptane adsorption on FCC catalyst/silicalite, Chem. Eng. Sci. 58 (2003) 2777–2784.
- [42] E. Ochoa-Fernández, T. Zhao, M. Rønning, D. Chen, Effects of steam addition on the properties of high temperature ceramic acceptors, J. Environ. Eng. 135 (2009) 397–403.
- [43] H.T.J. Reijers, S.E.A. Valster-Schiermeier, P.D. Cobden, R.W. van den Brink, Hydrotalcite as CO₂ sorbent for sorption-enhanced steam reforming of methane, Ind. Eng. Chem. Res. 45 (2006) 2522–2530.
- [44] E. Glueckauf, J.I. Coates, 241. Theory of chromatography. Part IV. The influence of incomplete equilibrium on the front boundary of chromatograms and on the effectiveness of separation, J. Chem. Soc. (1947) 1315–1321.

